X-ray spectroscopy for the magnetic study of the van der Waals ferromagnet $CrSiTe_3$ in the few- and monolayer limit

2D Materials

OPEN ACCESS

RECEIVED
13 May 2022

REVISED
20 June 2022

ACCEPTED FOR PUBLICATION
23 June 2022

PUBLISHED
7 July 2022

PAPER

X-ray spectroscopy for the magnetic study of the van der Waals ferromagnet $CrSiTe_3$ in the few- and monolayer limit

Ryuji Fujita[1], Jieyi Liu[1], Xiaofei Hou[2], Yanfeng Guo[2], Javier Herrero-Martín[3], Gerrit van der Laan[4] and Thorsten Hesjedal[1,*]

[1] Clarendon Laboratory, Department of Physics, University of Oxford, Parks Road, Oxford OX1 3PU, United Kingdom
[2] School of Physical Science and Technology, ShanghaiTech University, Shanghai 201210, People's Republic of China
[3] ALBA Synchrotron, Carrer de la Llum 2-26, 08290 Cerdanyola del Vallès, Barcelona, Spain
[4] Diamond Light Source, Harwell Science and Innovation Campus, Didcot, Oxfordshire OX11 0DE, United Kingdom
[*] Author to whom any correspondence should be addressed.

E-mail: Thorsten.Hesjedal@physics.ox.ac.uk

Keywords: x-ray absorption spectroscopy, x-ray magnetic circular dichroism, 2D van der Waals magnets, dimensionality, magnetization curve, thickness-dependent magnetic properties

Abstract

The study of magnetic order in few- and monolayer van der Waals materials poses a challenge to the most commonly employed magnetic characterization techniques as they normally lack magnetic sensitivity and/or lateral resolution enabling their thickness-dependent probing. Here we demonstrate the usefulness of x-ray absorption spectroscopy (XAS) and x-ray magnetic circular dichroism (XMCD) measurements, carried out at the Cr $L_{2,3}$ and Te M_5 edges, for the study of the ferromagnetic semiconductor $CrSiTe_3$ (CST) in the form of single- and few-layer flakes. By scanning the sample under the incident x-ray beam, a map of the exfoliated system was obtained, which reproduced the optical micrographs showing the detailed distribution and thicknesses of the flakes. In this way, XAS/XMCD was performed at selected sample areas, revealing the thickness-resolved spectroscopic and magnetic properties of the flakes, such as the spin and orbital magnetic moments. The spin moment, in line with the saturation field, is decreasing with film thickness, revealing a single-domain and out-of-plane magnetization for the thinnest films. For CST, the electronic properties are governed by the strong covalent bond between the Cr $3d(e_g)$ and Te $5p$ states, giving rise to a superexchange scenario. We observed a gradually increasing ratio of orbital to spin moment for thinner flakes, which could be due to a further increase of the covalent mixing. Hysteresis loops were recorded at the Cr L_3 edge, showing an open loop for 10 down to ~3 layers, while the bulk shows a wasp-waist shaped loop. With the transition temperature from the soft to the hard ferromagnetic state decreasing with thickness, the monolayer shows a narrowed, closed loop at 10 K, suggesting its transition temperature >10 K. Our study demonstrates the unique capabilities of XAS/XMCD for the study of few-layer van der Waals magnets, highlighting the interplay between electron correlation and ferromagnetism in CST.

1. Introduction

The recent discovery of long-range ferromagnetic order in atomically thin crystals has proven to be a key development in the field of two-dimensional (2D) materials, adding magnetic functionalities to the van der Waals (vdW) materials family [1–3]. These vdW materials, which often display novel behaviors in their standalone form, can also be stacked together into vdW heterostructures [4, 5], offering novel and unique attributes such as the switching of the magnetic state via pressure tuning [6, 7]. Moreover, owing to their 2D nature, the manipulation of magnetic order via external stimuli is in general very effective, and electrical [8] and optical [9] switching has been experimentally demonstrated. However, the control of the domain structure and density in such 2D magnets has yet to be demonstrated, while the Curie temperature (T_C) of monolayer magnets is still typically below an application-incompatible value of ~200 K

(taking the 2D ferromagnet 1 T-$CrTe_2$ with a bulk T_C of 310 K as an example [10]). As the magnetic order in 2D systems is relying on the presence of magnetocrystalline anisotropy [11, 12], thereby defeating the fluctuation-induced fate captured by the Mermin-Wagner theorem [13], common heterostructure engineering and doping may aid the effort of increasing T_C. Further, materials with a large intrinsic anisotropy such as Fe_3GeTe_2 [1, 3], but also Fe-rich Fe_5GeTe_2 [14–16], are recent examples. Exfoliable few- and monolayer compounds with above room temperature T_C and a tunable domain structure will certainly play an indispensable role in developing atomically thin magnetic device stacks, which could keep magnetic device scaling progressing further.

Semiconducting magnets, such as $CrSiTe_3$ (CST) [17–19] or monolayer $Ni(NCS)_2$ [20], are interesting members of the family of vdW magnets since in semiconductors, apart from their electronic properties, also the magnetism can be precisely tuned via electrical gating [21], making them ideal materials for spintronics applications. The magnetic properties of CST have been found to be strongly thickness dependent, which is common to all 2D magnets, however, with a rather unique increase (instead of the usual decrease) in the magnetic transition temperature as the films approach the monolayer limit [22, 23]. Note, however, that this conclusion is based on Hall measurements, whereas magneto-optical Kerr microscopy (MOKE) shows the opposite trend [24], in line with the findings for other 2D magnets [25]. This discrepancy, as well as the observation of topological magnetism, is often tied to changes of the local crystal structure, e.g. stemming from oxidation [26]. While MOKE is allowing for *in situ* studies of unoxidized flakes (in a glovebox), including temperature-dependent measurements and hysteresis loops, transport studies require patterned devices, which is usually exposing the flakes to air in the process. Despite the usefulness of MOKE for ultrathin 2D materials [3], a key issue remains, i.e. the strong reduction in magnetic sensitivity as the layer thickness approaches the monolayer limit. Further, MOKE is not an element-selective probe, making detailed studies of engineered heterostructures consisting of different 2D layers impossible.

X-ray absorption spectroscopy (XAS) and x-ray magnetic circular dichroism (XMCD) are element-specific, synchrotron-based techniques which provide a direct way to determine the local electronic and magnetic structure of 3*d* transition-metal atoms due to their valence-, site-, and symmetry-selectivity [27–30]. These capabilities make them ideally suited for the study of 2D magnets, allowing for the element-specific determination of spin and orbital moments. In fact, the bulk properties of Fe_3GeTe_2 [31], Fe_3GeTe_2/CrSb [32], and CST [33] have been studied, identifying unique features and details of the magnetic coupling mechanism, such as hybridization mediated superexchange in case of CST, inaccessible to MOKE or other, non-spectroscopic characterization techniques. Nevertheless, the study of the thickness dependence of the magnetic properties of 2D magnets using XAS/XMCD had not been reported so far owing to the rather large area typically probed by soft x-rays of several 100 μm across. While focusing of x-rays is in principle possible using zone plates [34], allowing for magnetic x-ray microscopy with ~10 nm resolution [35], it is not readily available at XMCD beamlines in the presence of a sufficiently large applied magnetic field.

Here, we demonstrate that XAS/XMCD can be used to locate and spectroscopically measure selected areas of defined atomic layer thickness CST flakes by using a beam spot of 13 μm × 58 μm. The distribution of the large-area flakes, which have been prepared by exfoliation in an Ar filled glovebox, were mapped out by optical microscopy before being transferred into the ultrahigh vacuum (UHV) chamber at the beamline end station. Using the XMCD sum rules [36, 37], we determined the thickness dependence of the spin and orbital moments which, among other explanations, might be suggesting that the Cr–Te hybridization is gradually increasing for thin flakes approaching the monolayer limit. Both spin and orbital moment values decrease with lower thickness, and the reduction in total moment for few-layer flakes is due to the reduction in transition temperature with thinner layers. Likewise, the magnetic hysteresis loops exhibit a distinct thickness dependence, with the bulk-like flake showing a wasp-waist shape with a nearly vanishing remanence. For thinner flakes, a clear ferromagnetic open-loop behavior is observed. As the transition temperature is significantly decreasing with layer thickness, the monolayer shows a closed loop at a measurement temperature of 10 K. As XMCD is a probe for the electronic structure of Cr and insensitive to structural changes beyond the nearest neighbors, the observed layer-dependence of the magnetization saturation is therefore a long range order effect.

2. Methods

2.1. $CrSiTe_3$ sample preparation

CST crystallizes in the $R\bar{3}$ space group, and is composed of ~3.5 Å thick Te-(Cr,Si)-Te layers, which are separated by a ~3.3 Å wide vdW gap between the Te layers, and stacking up in an A-B-C order to form the unit cell [18, 38]. The crystals readily cleave across the *c*-plane oriented vdW gaps. The CST flakes were prepared by exfoliation from well-characterized bulk crystals (which were subject of previous studies [33, 39, 40]) in an Ar-filled glovebox (O_2 and H_2O concentrations below 1 ppm) using a Au-assisted method [41] which yields large-area, *n* layer (*n*L) flakes on SiO_2/Si (figure 1). The flake thicknesses were determined *in situ* via

their optical contrast (figure 1(a)), which was cross-calibrated using *ex situ* atomic force microscopy (AFM) (see inset to figure 1(a)). After preparation, the samples were loaded directly into the UHV chamber without exposing them to air (base pressure $< 1 \times 10^{-10}$ mbar). The magnetic transition temperature of the bulk crystal was 32.8 K, as determined by superconducting quantum interference device magnetometry [33], and consistent with the value reported in the literature [17, 18, 42]. For the bulk crystal, we previously reported a saturation moment of 3.08 μ_B (at 2 K) [33], consistent with the value of 3 μ_B expected for Cr^{3+} with three unpaired spins [18]. The magnetic behavior of CST is best captured by a 2D Ising model coupled with long-range interaction, as concluded from a study of the critical behavior of the magnetic phase transition [43].

2.2. X-ray absorption and magnetic circular dichroism

XAS and XMCD measurements were carried out in the HECTOR end station on beamline 29 (BOREAS) at the ALBA Synchrotron in Barcelona, Spain [44]. At BOREAS, the beam size could be reduced down to 13 μm $\times$ 58 μm (full width at half maximum), allowing for layer-resolved magnetic spectroscopy by raster-scanning the sample. XAS spectra across the Cr $L_{2,3}$ (570–590 eV) were recorded with left- and right-circularly polarized (LCP and RCP) x-rays at normal incidence in a field of ± 6 T applied along the beam. The XAS signal, I_{sum}, is defined as $I^- + I^+$ with $I^- = \frac{1}{2}[I_{LCP}(H) + I_{RCP}(-H)]$ and $I^+ = \frac{1}{2}[I_{RCP}(H) + I_{LCP}(-H)]$, while the XMCD signal is $I_{xmcd} = I^- - I^+$ [30]. The measurements were carried out in total-electron yield detection mode, which is sensitive to the upper 3–5 nm of the sample [30], at a temperature of 10 K (unless otherwise stated). The photon energy was calibrated by measuring a Cr_2O_3 reference sample. This reference sample further allows for the verification of the pristine (unoxidized) CST sample state [45], which was found to remain unoxidized for the entire duration of the measurements.

The spin and orbital magnetic moments for Cr are determined by carrying out the sum rule analysis [46]. By integrating the XMCD spectra over the L_3 and $L_{2,3}$ edges, obtaining the values p and q, respectively, and by integrating I_{sum} over the $L_{2,3}$ edge to obtain the normalization factor r accounting for the number of d holes $n_h = 10 - n_d$, the spin and orbital moments per Cr atom are obtained as: $m_L = -\langle L_z \rangle = -(4/3)qn_h/r$ and $m_S = -\langle 2\ S_{eff,z} \rangle = -(6p - 4q)Cn_h/r$ [30]. Here, $C = 2$ is a correction factor for Cr [47]. The effective spin moment $\langle 2\ S_{eff,z} \rangle = \langle 2\ S_z \rangle + \langle 7\ T_z \rangle$, where $\langle 2\ S_z \rangle$ is the isotropic spin moment and $\langle T_z \rangle$ is the z component of the magnetic dipole term $\mathbf{T} = \sum_i \mathbf{s}_i - 3\ \hat{\mathbf{r}}_i(\hat{\mathbf{r}}_i \cdot s_i)$, where $\mathbf{s}_i$ and $\hat{\mathbf{r}}$ are the spin and position vector of the ith electron in the atom [37]. The tensor $\mathbf{T}$ gives the anisotropy of the spin moment due to the coupling of the spin with the charge quadrupole moment, which vanishes in the case of a cubic environment with negligible spin-orbit interaction, but can be non-zero otherwise.

The atomic multiplet calculation of the Cr $L_{2,3}$ XAS and XMCD spectra for the electric-dipole transitions $3d^n \rightarrow 2p^5 3d^{n+1}$ in bulk CST is reported in [33]. In bulk CST, we found a vanishing magneto-crystalline anisotropy and long-range ferromagnetism arising from superexchange [33], in agreement with (dynamical) mean-field theory calculations [39].

3. Results

The exfoliated few-layer CST flakes of constant thickness shown in the optical micrograph in figure 1(a) are typically >100 μm wide, and can therefore be selectively probed by XAS/XMCD. The optical micrographs were taken in an Ar-filled glovebox which is directly attached to the load-lock system of the end station, prior to the XAS/XMCD measurements. The optical contrast is a direct measure of the thickness of the layers (as indicated in figure 1(a) for 1, 3, 5, 6, and 10 L), and it is cross-calibrated by performing ex situ AFM measurements of the step heights, i.e. a specific optical contrast (color) corresponds to a particular n-layer thickness. One CST monolayer measures ~0.7 nm in thickness and the AFM image in the inset to figure 1(a) shows a two-layer step (from 1 to 3 L), amounting to 1.4 nm. Figure 1(b) shows the corresponding map of the magnetic asymmetry, defined as the difference of the XAS at the Cr L_3 edge obtained for opposite photon helicities, $\sigma_+ - \sigma_-$, at a fixed field. The asymmetry is changing with the number of layers. As can be seen, the contours of the nL flakes are reasonably well reproduced, allowing for the selective probing of these areas by positioning the x-ray beam at the desired spot.

Next, we carried out XAS and XMCD measurements on sample spots selected by thickness at 2 K and with a 3 T field applied out-of-plane. Figure 2(a) shows the normalized (to the maximum intensity at resonance) XAS data for 1, 3, 10 L, and a bulk-like area of the sample. All XAS spectra are very similar in shape, although they display small deviations in the pre-edge region of the Cr L_3 edge, and at the higher-energy edge of the L_2 edge, for the different thicknesses (highlighted in the zoomed-in insets). On the other hand, the XMCD spectra (normalized to the XAS intensity) show a strong thickness dependence of the intensity with the strongest dichroism for the bulk-like flake, and decreasing dichroic signals with decreasing flake thickness. From the inset to the XAS spectra in figure 2(a), it is seen that the small shoulder at the onset of the L_3 edge gains intensity for thinner layers. In figure 2(b), the XMCD spectra (normalized to their respective maxima) for the flakes are shown and compared with the theoretical multiplet spectrum for CST, as well as with the experimental

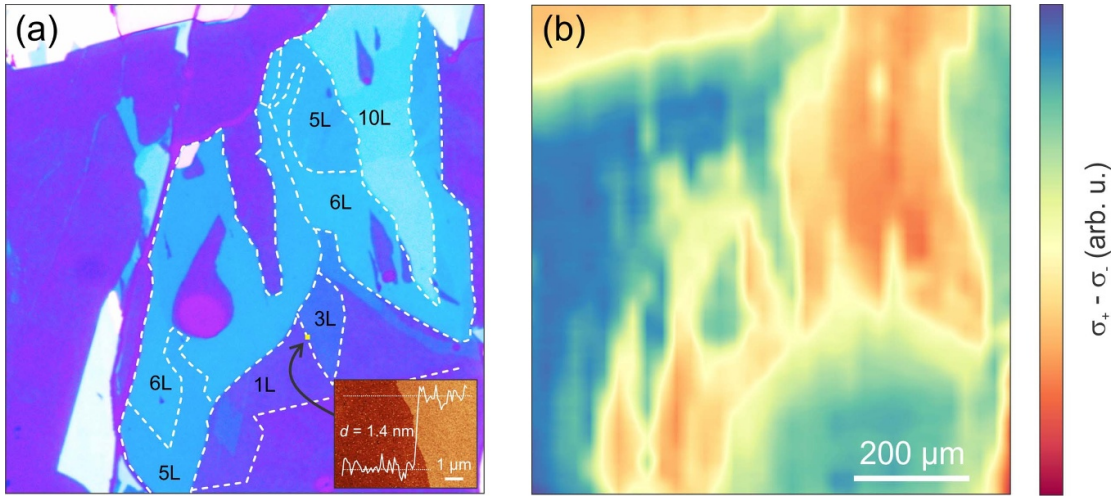

Figure 1. (a) Optical micrograph of few-layer CST flakes. Their n layer (nL) thickness correlates directly with the optical contrast, and can be further calibrated by atomic force microscopy (inset: height profile of a 1 L → 3 L step). Some boundaries of areas of identical thickness are indicated by dashed lines. (b) Spatial map of the magnetic asymmetry (at the Cr L_3 edge; taken at 10 K in zero applied field) of the same area as in (a), showing that the magnetic contrast is correlated with the thickness. The 200 μm scale bar applies to both panels.

spectra of a CST and a $CrGeTe_3$ bulk sample. The presence of a nonzero XMCD signal at the Te M_5 edge in both CST and $CrGeTe_3$ confirms a Te 5p spin polarization due to mixing with the Cr e_g bonding states. The results strongly suggest that superexchange, instead of the previously suggested single-ion anisotropy, is responsible for the low-temperature ferromagnetic ordering in both 2D materials [33]. Looking at the XMCD in figure 2(b), no noticeable change in the relative Te M_5 intensity as a function of layer thickness is evident.

Next, we determined the orbital and spin moments, m_S and m_L, for different layer thicknesses at 3 T field using the XMCD sum rules [30, 36, 37] for the bulk layer, and scaling of m_L with $(A_3 + A_2)$ and m_S with $(A_3 - 2A_2)$, where A_3 and A_2 are the integrated areas underneath the L_3 and L_2 peaks in the XMCD spectrum, respectively. Note that A_2 and A_3 have opposite signs, owing to the fact that spin and orbit are coupled opposite for the $p_{3/2}$ and $p_{1/2}$ core levels. For the bulk sample (taking the number of 3d electrons $n_d = 3.5$), we obtain from the orbital and spin sum rules $m_L = -0.055\,\mu_B$/Cr and $m_S = 2.86\,\mu_B$/Cr, agreeing well with our earlier observations on cleaved bulk samples of $m_L = (-0.055 \pm 0.05)\,\mu_B$/Cr and $m_S = (2.86 \pm 0.25)\,\mu_B$/Cr [33]. For the thinner flakes the corresponding magnitudes of the moments monotonically decrease with thickness as shown in figure 3 and summarized in table 1. The spin moment, and thereby the saturation field, are strongly decreasing for thinner samples (figure 3(a)).

Finally, using the XMCD signal we measured the magnetic hysteresis of the different flakes, in out-of-plane fields ranging from −0.25 to 0.25 T at a temperature of 10 K. Figure 4 shows the loops for decreasing CST thickness (from top to bottom) on the same (arbitrary) intensity scale. Note that the XMCD signal in TEY detection mode at low fields tends to be noisy as the electrons escaping from the surface will be affected by the reduced applied field. The hysteresis loop of bulk CST measured by XMCD at 10 K in figure 4 shows a wasp-waist shape with a near vanishing remanence. This soft ferromagnetic behavior is in agreement with earlier reports [18], that found no hysteretic behavior and a negligible remanent magnetization. Note that magnetic susceptibility measurements on the bulk CST single crystal reveal a paramagnetic-to-ferromagnetic phase transition at a Curie temperature of 32.8 K with the easy-axis along the c-axis [24, 33]. The wasp-waist shape is due to the range of domain sizes with different magnetic orientations. These loops are a mixture of a steeper Langevin function and more open hysteresis curves of the blocked domains with different orientations [24, 49, 50].

4. Discussion

We will first discuss the strong changes observed in both m_S and the saturation magnetization as a function of layer thickness, and then discuss the observed small changes in m_L/m_S.

4.1. Saturation magnetization and spin moment

The experimental results on CST, summarized in table 1, show a decrease in spin moment, i.e. a decrease of saturation field for thinner samples, which is confirmed by the hysteresis loops in figure 4. In contrast to the zero-remanence loop for bulk CST, the loops of the thin layers show a remanent field. Likewise, the saturation magnetization shows a clear thickness dependence. As can be seen from table 1, the

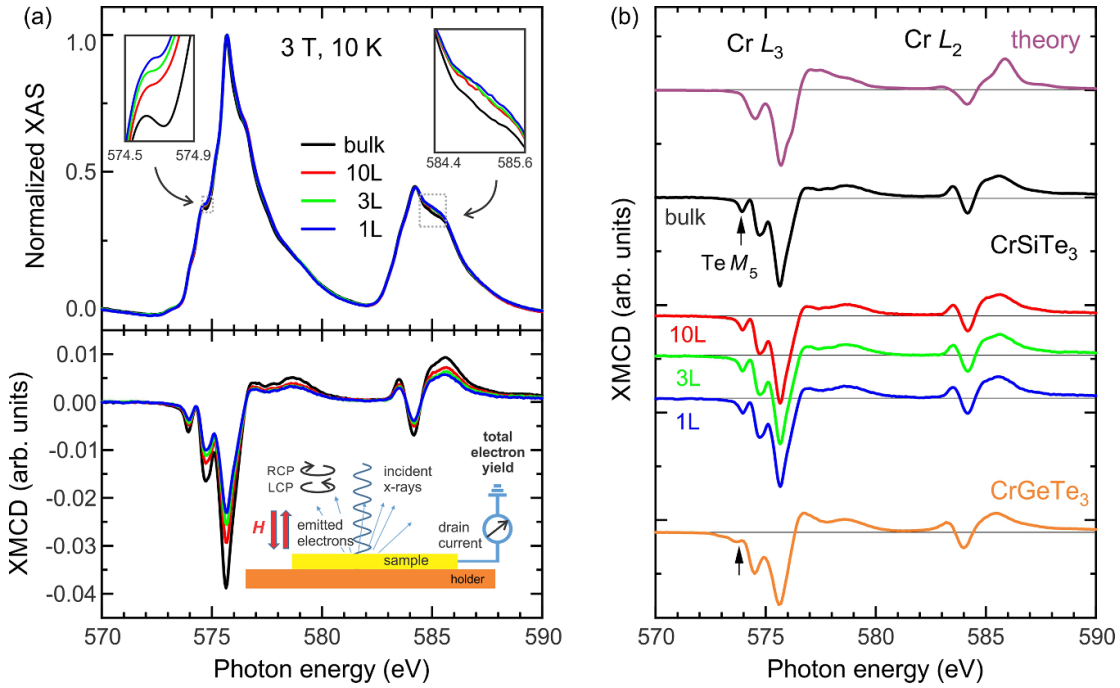

Figure 2. (a) Cr $L_{2,3}$ x-ray absorption spectroscopy (XAS) and XMCD data of $CrSiTe_3$ (CST) flakes of defined thickness obtained at 10 K in an applied field of 3 T. The inset below shows the experimental geometry with x-rays under normal incidence and the applied field along the beam. In total electron yield (TEY) mode, the drain current is recorded. In the XAS data (above), there is overall a weak thickness dependence of the spectra observable. There are some notable thickness dependence energy windows, which are shown as insets to panel (a) and whose locations are marked up by dotted lines. In contrast, the XMCD signals (below) scaled to the corresponding XAS, show a clear thickness dependence due to changes in the saturation magnetization, as discussed in the text. (b) Comparison of the theoretical multiplet spectrum at the Cr $L_{2,3}$ edge for CST with the experimental XMCD spectra for bulk CST (black), 10 L (red), 3 L (green), and a 1 L flake (blue). Note that the CST spectra have been normalized to their respective maxima and appear rather similar in spectral shape. For comparison, the experimental spectrum for $CrGeTe_3$ is shown below (orange) [48]. The position of the Te M_5 peak is labeled by black arrows, indicative of hybridization between Cr and Te.

spin moment gradually decreases for thinner layers, and for 1 L it is reduced by 60% compared to the bulk value. The reason for this is that the Curie temperature strongly decreases with the film thickness. For 10 L the T_C is still close to the bulk value of 32.8 K, however, at 10 K a ferromagnetic-to-paramagnetic transition occurs for films below 4.6 nm, i.e. 6–7 L [24].

This means that the demagnetization field changes at the critical thickness, which directly influences the domain structures, domain walls, and nucleation of reversed domains. For the thinner films it demonstrates a single-domain, highly anisotropic out-of-plane spin polarization. However, in this case, the saturation field is lower than that of the bulk due to the decreased transition temperature. For the thinner samples at 10 K (figure 4), the coercivity of the hysteresis loop is smaller for the 3 L flake compared to the 10 L one, and it becomes negligible for the 1 L flake. For the latter, the XMCD signal shows a linear relationship with the applied field, suggesting that long-range ferromagnetic order is absent at 10 K. The samples in the nm thickness range are too thin to support a domain wall.

From DFT calculations, the domain wall thickness was estimated to be ~10 nm [51]. Therefore, when the thickness is below the typical domain wall size of 10 nm, domain formation will be suppressed, consistent with the presence and absence of the maze-shaped domain in bulk and thin samples in our experimental observation, respectively [24]. Moreover, from an energetic point of view, ferromagnetic domains arise from the minimization of the stray field energy. In bulk CST, since the stray field energy is larger than the energy required to form domain walls, the ferromagnet will break up into domains. However, as the thickness decreases, the saturation field decreases as shown in figure 4 and table 1, as well as the magnetization and stray field.

The thickness dependent behavior indicates a crossover from 3D to 2D Ising ferromagnetism, which is often observed in ultrathin layered magnets, such as 2D magnets Fe_3GeTe_2 [3]. An alternative explanation for the layer-dependent magnetic properties would be a structural transition or distortion as the thickness decreases, as reported for CrI_3 [52].

4.2. Orbital to spin moment ratio

To understand the orbital character of the valence electrons and hybridization, the orbital magnetic moment should be taken into account.

The ratio of m_L over m_S is an important indicator for the electronic and magnetic properties as several

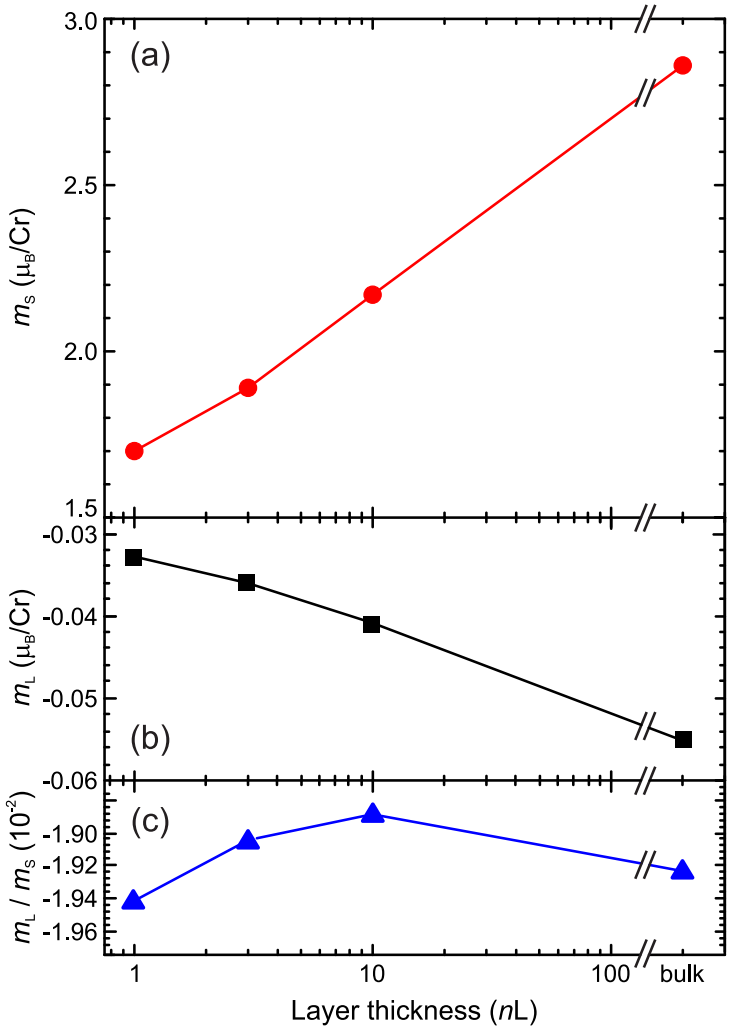

Figure 3. (a) Spin and (b) orbital magnetic moments of Cr in CST (extracted using the sum rules) vs flake thickness measured at 10 K and in an applied out-of-plane field of 3 T. (c) The ratio of orbital to spin moment, m_L/m_S, increases gradually in magnitude from 10 L to 1 L.

Table 1. Summary of the Cr spin and orbital moments for the different layer thicknesses.

	1 L	3 L	10 L	Bulk
m_S (μ_B/Cr)	1.7	1.89	2.17	2.86
m_L (μ_B/Cr)	−0.033	−0.036	−0.041	−0.055
m_L/m_S (10^{-2})	−1.94	−1.91	−1.89	−1.92

effects, such as the number of holes and the changing saturation of the field, cancel out in this ratio. In other words, it normalizes the orbital moment to the spin moment. In the plot of m_L/m_S (figure 3(c) and table 1), it can be seen that its magnitude is slowly increasing for thinner films below 10 L. The weak orbital moment is coupled to the spin moment by the 3*d* spin–orbit coupling, and follows the same trend as the spin moment. The opposite sign of the spin and orbital moment is expected from the third Hund's rule as they are aligned antiparallel for less than half-filled shell.

From table 1, we see that, although m_L/m_S remains close to −0.019, it gradually increases by 2.5% for 10 L to 1 L. Such an increase in the m_L/m_S ratio can have several different origins: (a) an increase in the perpendicular magnetic anisotropy for thinner layers, since the easy direction of magnetization always has the largest orbital moment [30], (b) a change in the value of $\langle T_z \rangle$, which appears as part of m_S, and/or (c) an increase in the amount of e_g character in the 3*d* wavefunction. We cannot readily dismiss any of these origins, or a combination of them. The absolute value of $\langle T_z \rangle$ can be larger for an ultrathin film as the high symmetry of the bulk is broken [53], but this is difficult to quantify without advanced bandstructure calculations. It is plausible that for thinner layers the

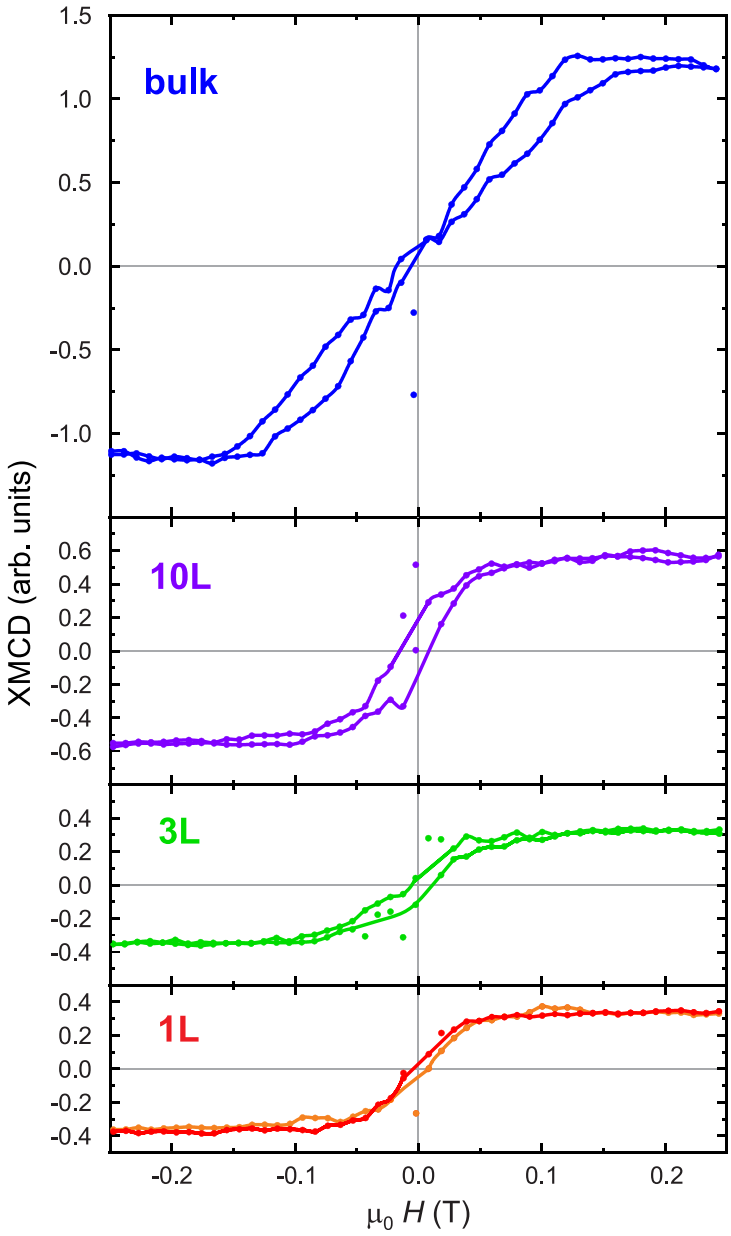

Figure 4. Cr-XMCD hysteresis loops of a bulk-like, a 10 L, 3 L, and 1 L $CrSiTe_3$ flake (from top to bottom), measured at 10 K. The bulk-like flake shows a loop opening at non-zero fields. The loop is also fully open for the 10 L and 3 L flakes, while the 1 L loop is nearly closed. The loops of the thicker layers are generally more rounded and their saturation fields are larger compared to the 1 L loop. Note that the solid lines represent a rolling average over the measured data points, omitting the low-field data points which are typically noisy when measuring in TEY mode.

Cr–Te hybridization becomes stronger. In a recent XAS/XMCD study on bulk CST, Achinuq *et al* [33] concluded that in Cr, besides t_{2g}^3 with zero orbital moment, there is also a small fraction of e_g electrons, which contribute an orbital moment. The Cr e_g electrons hybridize with the Te 5*p* band. This hybridization is corroborated by the presence of a Te M_5 peak in the XMCD, evidencing spin polarized holes in the Te 5*p* band. The inset of figure 2(a), top panel, shows a higher signal at the onset of the Cr L_3 XAS for thinner layers, but this is not clearly accompanied by a corresponding change in the XMCD spectral shape. On the other hand, figure 2(a) shows that the Cr L_3 spectrum gains intensity in the region 576.5–580 eV and the L_2 spectrum gains intensity in the 585–587 eV region. If we were to switch on the hybridization in the multiplet calculation, the intensity increases at the high energy sides of the absorption peak (roughly those parts that are positive in the XMCD). Thus, the increased m_L/m_S ratio might suggest an increase in hybridization for lower film thickness. It is fair to say that we cannot draw hard conclusions from the small change in m_L/m_S, other than that none of these above-mentioned effects can be very strong.

5. Conclusion

We have demonstrated that XAS/XMCD is a useful technique for the layer thickness-dependent study of 2D magnets. By using a small spot size of the probing x-ray beam of $\sim$13 μm $\times$ 58 μm, in combination with large, well-defined flakes exfoliated in an attached glovebox, we obtained the orbital and spin magnetic moments of Cr in CST flakes as a function of *n*L thickness. The spin and orbital moments, as well as their combined total moment, are decreasing in magnitude with lower layer thickness. The decrease in spin moment, and thereby the saturation field, is directly related to the domain structure of very thin layers, which exhibit a highly anisotropic, out-of-plane single-domain state. The XMCD sum rule analysis revealed a small increase in the ratio of orbital to spin moment with decreasing thickness below 10 L, for which we provided possible reasons, including an increase of covalency for thinner flakes. The magnetic hysteresis loops also exhibit a distinct thickness dependence, with the bulk-like flake showing a wasp-waist shape with a near vanishing remanence. For thinner flakes, a clear ferromagnetic open-loop behavior is observed. As the transition temperature from the soft to the hard ferromagnetic state strongly decreases with layer thickness, the monolayer shows no open loop at a measurement temperature of 10 K. As XMCD is a probe for the local electronic structure of Cr, and therefore insensitive to structural changes beyond the nearest neighbors, the observed layer-dependence of the magnetization saturation is therefore a long range order effect.

In the future, we will carry out detailed measurements of the transition temperatures and magnetic critical behavior of CST flakes, as well as other 2D magnets and heterostructures, via an Arrott-Noakes analysis based on temperature-dependent hysteresis curves [54], which is also a viable, yet time-consuming route using XMCD [55]. By determining the critical exponents, the possible transition from 3D to 2D magnetic coupling, if present, will be observable, as each common model, i.e. the 2D Ising model, the 3D Heisenberg model, the 3D Ising model, the 3D XY model, and the tricritical mean-field model, has its unique set of critical exponents [56]. By being able to both carry out the exfoliation and do optical characterization of the sample in an Ar glovebox which is attached to the load-lock of the beamline's end station, pristine and unoxidized flakes of defined thickness can be probed.

Data availability statement

All data that support the findings of this study are included within the article (and any supplementary files).

Acknowledgments

These experiments were performed at the BOREAS beamline at the ALBA Synchrotron (proposal 2021025032). Y F G acknowledges the open projects from State Key Laboratory of Surface Physics and Department of Physics, Fudan University (Grant No. KF2020_09) and National Laboratory of Solid State Microstructures, Nanjing University (Grant No. M34015). R F and T H acknowledge financial support from the Oxford-ShanghaiTech collaboration project and the UK Skyrmion Project (Engineering and Physical Sciences Research Council, EP/N032128/1).

Conflict of interest

The authors declare no competing financial interest.

ORCID iDs

Ryuji Fujita https://orcid.org/0000-0001-8557-5812
Jieyi Liu https://orcid.org/0000-0001-6588-5987
Yanfeng Guo https://orcid.org/0000-0002-9386-4857
Javier Herrero-Martín https://orcid.org/0000-0003-1986-8128
Gerrit van der Laan https://orcid.org/0000-0001-6852-2495
Thorsten Hesjedal https://orcid.org/0000-0001-7947-3692

References

[1] Gong C *et al* 2017 *Nature* **546** 265–9
[2] Huang B *et al* 2017 *Nature* **546** 270–3
[3] Fei Z *et al* 2018 *Nat. Mater.* **17** 778–82
[4] Withers F *et al* 2015 *Nat. Mater.* **14** 301–6
[5] Sierra J F, Fabian J, Kawakami R K, Roche S and Valenzuela S O 2021 *Nat. Nanotechnol.* **16** 856–68
[6] Li T *et al* 2019 *Nat. Mater.* **18** 1303–8
[7] Song T *et al* 2019 *Nat. Mater.* **18** 1298–302
[8] Jiang S, Shan J and Mak K F 2018 *Nat. Mater.* **17** 406–10
[9] Seyler K L *et al* 2018 *Nano Lett.* **18** 3823–8
[10] Meng L *et al* 2021 *Nat. Commun.* **12** 809
[11] Burch K S, Mandrus D and Park J-G 2018 *Nature* **563** 47–52
[12] Wei S, Liao X, Wang C, Li J, Zhang H, Zeng Y-J, Linghu J, Jin H and Wei Y 2021 *2D Mater.* **8** 012005
[13] Mermin N D and Wagner H 1966 *Phys. Rev. Lett.* **17** 1133–6
[14] May A F, Ovchinnikov D, Zheng Q, Hermann R, Calder S, Huang B, Fei Z, Liu Y, Xu X and McGuire M A 2019 *ACS Nano* **13** 4436–42
[15] May A F, Bridges C A and McGuire M A 2019 *Phys. Rev. Mater.* **3** 104401
[16] Chen H *et al* 2022 *2D Mater.* **9** 025017
[17] Carteaux V, Moussa F and Spiesser M 1995 *Europhys. Lett.* **29** 251–6
[18] Casto L D *et al* 2015 *APL Mater.* **3** 041515
[19] Carteaux V, Brunet D, Ouvrard G and Andre G 1995 *J. Phys.: Condens. Matter* **7** 69–87
[20] Wu Y, Sun W, Liu S, Wang B, Liu C, Yin H and Cheng Z 2021 *Nanoscale* **13** 16564–70
[21] Dietl T and Ohno H 2014 *Rev. Mod. Phys.* **86** 187–251

[22] Williams T J, Aczel A A, Lumsden M D, Nagler S E, Stone M B, Yan J-Q and Mandrus D 2015 *Phys. Rev.* B **92** 144404
[23] Lin M-W *et al* 2016 *J. Mater. Chem.* C **4** 315–22
[24] Zhang C *et al* 2022 *Nanoscale* **14** 5851–8
[25] Ningrum V P *et al* 2020 *Research* **2020** 1768918
[26] Park T-E *et al* 2021 *Phys. Rev.* B **103** 104410
[27] van der Laan G and Thole B T 1991 *Phys. Rev.* B **43** 13401–11
[28] van der Laan G and Kirkman I W 1992 *J. Phys.: Condens. Matter* **4** 4189
[29] van der Laan G 2013 *J. Phys. Conf. Ser.* **430** 012127
[30] van der Laan G and Figueroa A I 2014 *Coord. Chem. Rev.* **277–278** 95–129
[31] Li Q *et al* 2018 *Nano Lett.* **18** 5974–80
[32] Liu S *et al* 2020 *Natl. Sci. Rev.* **7** 745–54
[33] Achinuq B, Fujita R, Xia W, Guo Y, Bencok P, van der Laan G and Hesjedal T 2022 *Phys. Status Solidi* **16** 2100566
[34] Di Fabrizio E, Romanato F, Gentili M, Cabrini S, Kaulich B, Susini J and Barrett R 1999 *Nature* **401** 895–8
[35] Jacobson C 2020 *X-ray Microscopy* (Cambridge: Cambridge University Press)
[36] Thole B T, Carra P, Sette F and van der Laan G 1992 X-ray circular dichroism as a probe of orbital magnetization *Rev. Lett.* **68** 1943–6
[37] Carra P, Thole B T, Altarelli M and Wang X 1993 *Phys. Rev. Lett.* **70** 694–7
[38] Milosavljević A, Šolajić A, Pešić J, Liu Y, Petrovic C, Lazarević N and Popović Z V 2018 *Phys. Rev.* B **98** 104306
[39] Zhang J *et al* 2019 *Phys. Rev. Lett.* **123** 047203
[40] Suo P, Xia W, Zhang W, Zhu X, Fu J, Lin X, Jin Z, Liu W, Guo Y and Ma G 2020 *Laser Photonics Rev.* **14** 2000025
[41] Huang Y *et al* 2020 *Nat. Commun.* **11** 2453
[42] Carteaux V, Ouvrard G, Grenier J C and Laligant Y 1991 *J. Magn. Magn. Mater.* **94** 127–33
[43] Liu B, Zou Y, Zhang L, Zhou S, Wang Z, Wang W, Qu Z and Zhang Y 2016 *Sci. Rep.* **6** 33873
[44] Barla A, Nicolás J, Cocco D, Valvidares S M, Herrero-Martín J, Gargiani P, Moldes J, Ruget C, Pellegrin E and Ferrer S 2016 *J. Synchrotron Radiat.* **23** 1507–17
[45] Burn D M, Duffy L B, Fujita R, Zhang S L, Figueroa A I, Herrero-Martin J, van der Laan G and Hesjedal T 2019 *Sci. Rep.* **9** 10793
[46] van der Laan G 1998 *Phys. Rev.* B **57** 112
[47] Figueroa A I, van der Laan G, Collins-McIntyre L J, Zhang S-L, Baker A A, Harrison S E, Schönherr P, Cibin G and Hesjedal T 2014 *Phys. Rev.* B **90** 134402
[48] Watson M D *et al* 2020 *Phys. Rev.* B **101** 205125
[49] Tauxe L, Mullender T and Pick T 1996 *J. Geophys. Res.* **101** 571–83
[50] Dudzik E, Dürr H A, Dhesi S S, van der Laan G, Knabben D and Goedkoop J B 1999 *J. Phys.: Condens. Matter* **11** 8445–51
[51] Zhang C *et al* 2021 *Nano Lett.* **21** 7946–52
[52] Sun Z *et al* 2019 *Nature* **572** 497–501
[53] van der Laan G 1998 *J. Phys.: Condens. Matter* **10** 3239
[54] Arrott A and Noakes J E 1967 *Phys. Rev. Lett.* **19** 786–9
[55] Figueroa A, Baker A, Harrison S, Kummer K, van der Laan G and Hesjedal T 2017 *J. Magn. Magn. Mater.* **422** 93–99
[56] Gibertini M, Koperski M, Morpurgo A F and Novoselov K S 2019 *Nat. Nanotechnol.* **14** 408–19